

Contents lists available at ScienceDirect

Materials Letters

journal homepage: www.elsevier.com/locate/matlet





Laser cladding of CoCrFeNi high-entropy alloy coatings: Compositional homogeneity towards improved corrosion resistance

Qi Zhu, Yu Liu, Chunyang Zhang *

Central Hospital Affiliated to Shenyang AQ3 Medical College, Shenyang 110032, China

ARTICLE INFO

Keywords:
Laser cladding
Annealing
CoCrFeNi
High-entropy alloy coating
Compositional homogeneity
Corrosion resistance

ABSTRACT

Laser cladding of high-entropy alloy (HEA) coatings has aroused increasing attention in recent years. However, laser-cladded HEA coatings often suffer phase separation and/or elemental segregation, which may limit their full potential for corrosion resistance. In this study, CoCrFeNi HEA coatings were deposited on AISI 1045 steel substrate via laser cladding and then were subjected to post-annealing treatment. Microstructural characterization shows that a single-phase FCC structure forms in the laser-cladded CoCrFeNi HEA coating, without any phase separation. Columnar grains with cell substructures are dominating, with enrichment of Cr on cell walls and enrichment of Fe, Co, and Ni in cell interiors. Post-annealing promotes the recrystallization and the formation of equiaxed grained microstructures, and simultaneously erases the elemental segregation. Such homogenous elemental distributions lead to a higher corrosion potential and a lower corrosion current density, indicating an enhanced corrosion resistance. Such findings provide a guideline for fabricating highly corrosion-resistant HEA coatings for critical applications.

1. Introduction

High-entropy alloys (HEAs) are newcomers to the world of metallic materials. Deviating from conventional alloys with a single principal element, HEAs consist of multiple principal elements, with each at 5 to 35 at.% [1]. Multiple superior properties have been reported for HEAs, including excellent strength-ductility synergy [2] and excellent corrosion resistance [3], etc. Especially, excellent corrosive properties make HEAs promising coating materials [4–8]. Several coating techniques are available such as magnetron sputtering and plasma spraying. In contrast, laser cladding is a reliable coating technique which enables the fabrication of large-scale coatings [9]. The partial remelting of the substrate also facilitates the good substrate/coating metallurgical bonding. Recently, HEA coatings have been fabricated via laser cladding, which improves the corrosion resistance of the substrate materials [10,11]. However, phase separation in laser-cladded HEA coatings is frequently observed [12,13], despite the high configuration entropy of HEAs. For example, the laser-cladded Al_{0.5}FeCu_{0.7}NiCoCr HEA coating has a dual-phase (FCC plus BCC) microstructure [10]. Jiang et al. [13] also reported that TiZrAlNbCo HEA coating has a matrix phase of FCC plus BCC, as well as minor intermetallic phases. It is worth mentioning that BCC phases are preferentially corroded in such a multi-phase

microstructure. In addition to the phase separation, elemental segregation often occurs in the laser-cladded HEA coatings [14], despite high cooling rates of laser cladding and sluggish diffusion effects of HEAs. Such phase separation and elemental segregation phenomenon may limit the full potential for improved corrosion resistance of laser-cladded HEA coatings.

In this paper, CoCrFeNi HEA coatings were deposited on the AISI 1045 steel substrate via laser cladding and then were subjected to post-annealing treatment. The AISI 1045 steel has good comprehensive mechanical properties and low cost, but its corrosion resistance is normally insufficient. The CoCrFeNi HEA has been reported to have a single-phase FCC structure [15], possibly ensuring the good substrate/coating metallurgical bonding. Furthermore, the CoCrFeNi HEA has shown good laser processing ability, without any cracks [16]. Such characteristics make the CoCrFeNi HEA a promising coating material for the AISI 1045 steel substrate. Our findings show that the single-phase characteristics and homogenous elemental distributions of the laser-cladded and annealed CoCrFeNi HEA coatings result in the dramatically enhanced corrosion resistance.

E-mail address: Emergency_zhangcy@163.com (C. Zhang).

^{*} Corresponding author.

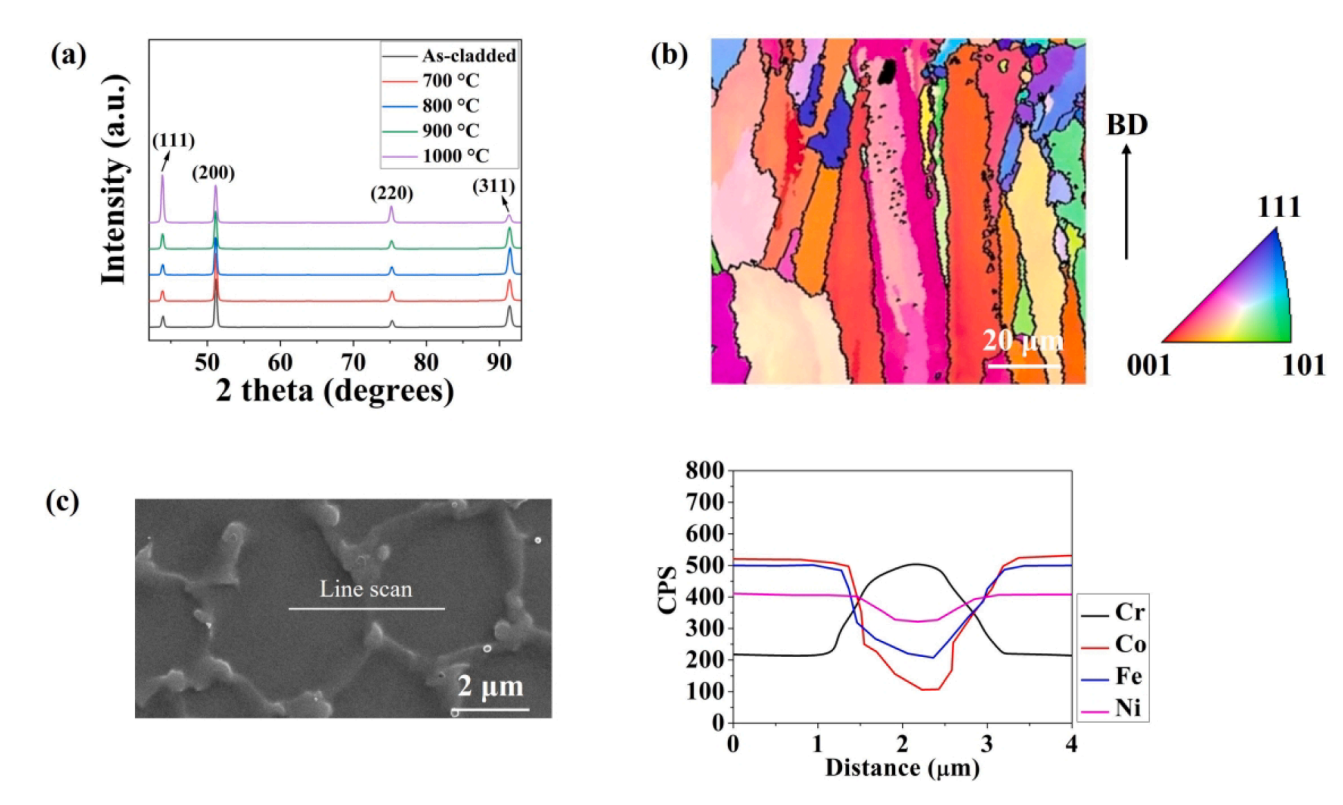


Fig. 1. (a) XRD patterns of the as-cladded and the annealed CoCrFeNi HEA coatings. (b) EBSD inverse pole figure (IPF) map of the as-cladded CoCrFeNi HEA coating. The building direction (BD) is the reference direction for the IPF map. (c) A typical SEM micrograph of cells, along with EDS line scan result, of the as-cladded CoCrFeNi HEA coating.

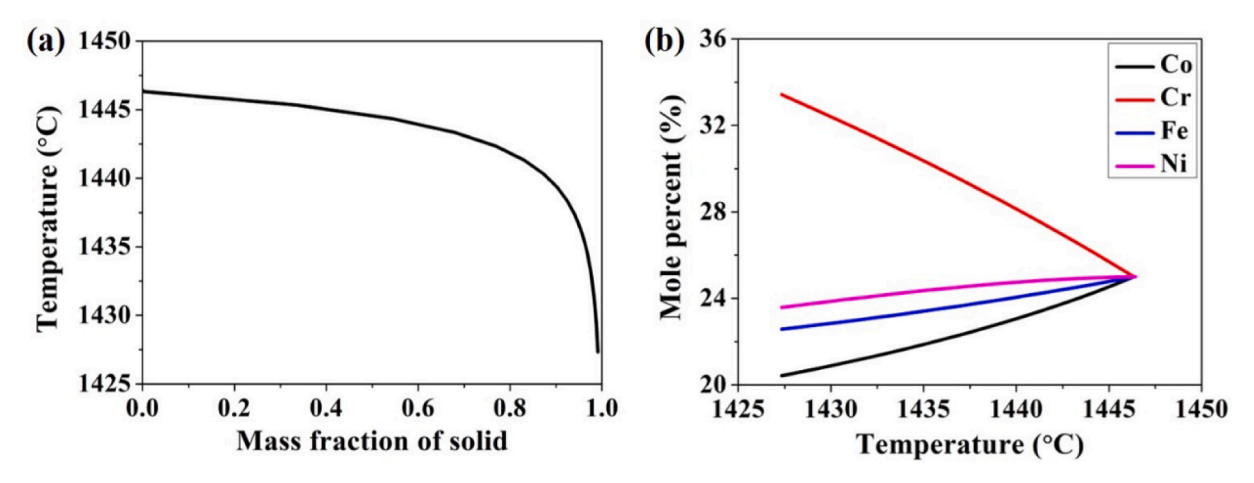


Fig. 2. Scheil simulation performed on the platform of Thermo-Calc software with the aid of HEA thermodynamic database. (a) Solidification path. (b) Compositional evolution of the molten alloy with temperature.

2. Experimental

The detailed information on the coating preparation, post-annealing treatment, microstructural characterization, electrochemical testing, and thermodynamic calculations was presented in Supplementary File.

3. Results and discussion

Fig. 1(a) shows the XRD patterns of the laser-cladded and the annealed CoCrFeNi HEA coatings. It can be seen that only disordered FCC peaks were indexed from the XRD patterns, and such a single-phase FCC microstructure is consistent with its counterparts by casting [17] or additive manufacturing [16,18]. Such a single-phase microstructure also

diverts from most existing HEA coatings that have phase separations [10,12,13]. There are no cracks and pores at the substrate/coating interface, indicating a good interfacial cohesion. Good interfacial cohesion can be attributed to the partial remelting and dilution of the AISI 1045 steel substrate (Fig. S1). EBSD mapping demonstrates that the laser-cladded CoCrFeNi coating is dominated by columnar grains rather than equiaxed grains (Fig. 1(b)). According to classic solidification theory, the grain morphology is concurrently determined by temperature gradient (G) and solidification velocity (R), and often the G values can reach $10^2 \sim 10^4$ °C/mm during laser-induced melt pool solidification [19]. Such a high G value normally facilitates the formation and subsequent epitaxial growth of columnar grains that can span over several deposition layers. Within the columnar grains, fine cell

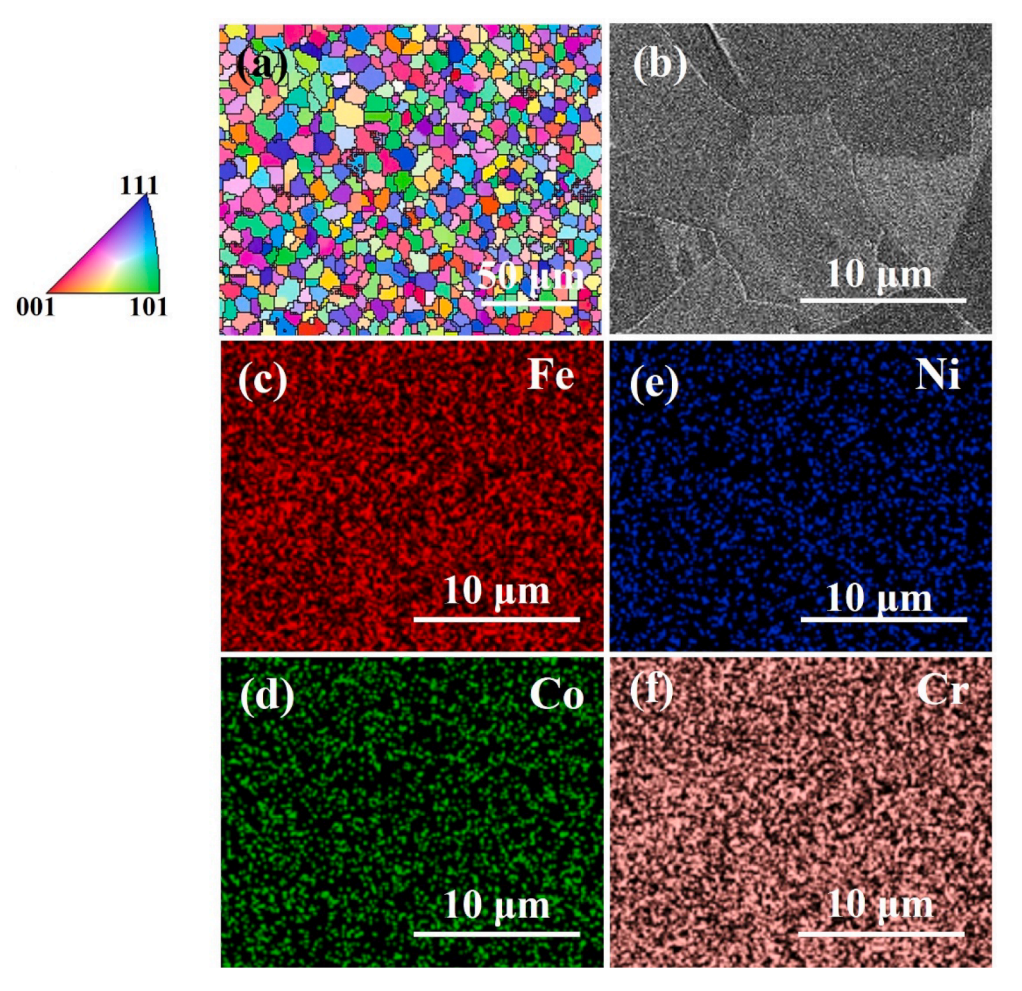


Fig. 3. (a) EBSD IPF map of the 1000 °C annealed CoCrFeNi coating. (b) A typical SEM micrograph and (c-f) corresponding EDS mapping results of the 1000 °C annealed CoCrFeNi coating.

structures were observed (Fig. 1(c)). Based on the EDS mapping, it was confirmed that the cell walls are enriched with Cr, whereas the cell interiors are enriched with Co, Fe, and Ni.

The phase constitution and elemental segregation of the lasercladded CoCrFeNi HEA coating are discussed with the aid of Scheil simulation. As can be seen from Fig. 2(a), a single FCC phase was predicted to solidify from the molten alloy, which supports our XRD results. Fig. 2(b) demonstrates that the remaining liquid is progressively enriched with Cr and depleted with Co, Fe, and Ni. This indicates that latter solidified regions, i.e., cell walls, are enriched with Cr, and depleted with Co, Fe, and Ni. Such predictions are consistent with the EDS result (Fig. 1(c)). It's worth noting, however, that the CoCrFeNi HEAs prepared by selective laser melting were reported to have a very homogeneous elemental distribution, without any elemental segregation [16,18]. This can be attributed to the extremely large cooling rate intrinsic to selective laser melting, which can reach up to $10^4 \sim 10^{\bar{7}} \, {}^\circ\text{C/s}$ [20]. In contrast, the cooling rate during laser cladding is not as pronounced as during selective laser melting, and hence the segregation kinetics can't be suppressed completely in our case.

To remove the elemental segregation, we performed post-annealing, i.e. holding at 700, 800, 900, 1000 $^{\circ}\text{C}$ for 2 hr followed by water quenching. Samples annealed at 700, 800, 900 $^{\circ}\text{C}$ are similar to what observed in the as-cladded CoCrFeNi coating, e.g., columnar grains, and cell structures (Fig. S2). This indicates that solidification segregation has not been removed, possibly due to sluggish diffusion effects of HEAs [21]. With the annealing temperature further increasing to 1000 $^{\circ}\text{C}$, the laser-cladded features were totally removed, as shown in Fig. 3. Firstly, the columnar grained microstructures in the laser-cladded coating were

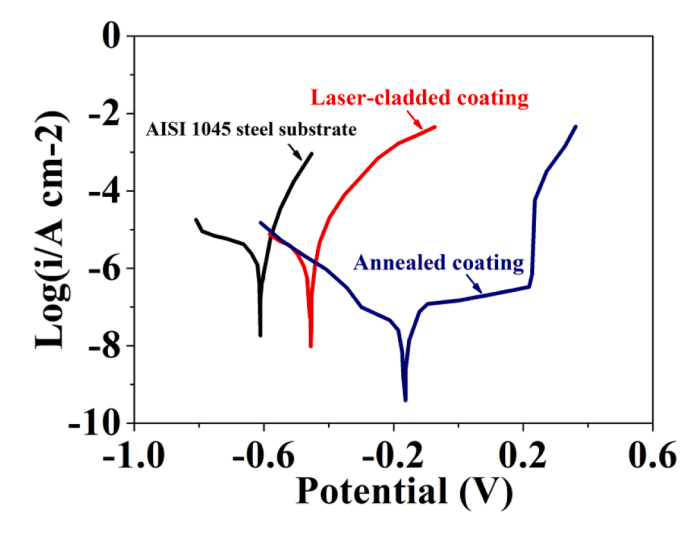


Fig. 4. Potentiodynamic polarization curves of AISI 1045 steel substrate and CoCrFeNi HEA coatings in both laser-cladded and annealed states.

totally replaced by the equiaxed grained microstructures (Fig. 3(a)). As we all know, the laser-cladded microstructures are often featured with large residual strains, and upon high-temperature annealing, a recrystallization process can occur by the nucleation and growth of equiaxed grains. Furthermore, the cell structures and elemental segregation were

also totally removed, as can be seen from Fig. 3(b-f).

Fig. 4 shows the potentiodynamic polarization curves of the AISI 1045 steel substrate as well as the CoCrFeNi HEA coatings in both lasercladded and annealed states. It can be seen that as compared with the AISI 1045 steel substrate, the corrosion potential of the laser-cladded CoCrFeNi coating is much higher. After 1000 °C annealing, the corrosion potential further increases to -0.168 V. The 1000 °C-annealed CoCrFeNi coating also shows a pronounced passive platform, i.e. the current does not change with the potential increase. The improved corrosion resistance of the laser-cladded CoCrFeNi HEA coating can be attributed to the following reason. The AISI 1045 steel often suffers from the pitting corrosion in the solution containing Cl⁻¹ ions. When we form a CoCrFeNi HEA coating by laser cladding, the high-entropy effect and the rapid solidification effect resulting from HEAs and laser cladding, respectively, enable us to achieve a simple single-phase FCC microstructure. Furthermore, the high Cr content in the CoCrFeNi HEA coating definitely facilitates the formation of the protective layer. When subjected to 1000 °C annealing, the elemental segregation in the CoCrFeNi HEA coating was totally removed. The homogenous distribution of elements (especially Cr) can make the protective layer more uniform and more protective. The findings of this paper provide the guidelines for fabricating corrosion-resistant HEA coatings.

4. Conclusions

The CoCrFeNi HEA coating was successfully deposited on the AISI 1045 steel substrate via laser cladding. The CoCrFeNi HEA coating has a single-phase FCC structure, without any phase separation. Columnar grained microstructures, cell structures as well as elemental segregation were observed. Specifically, the cell walls are enriched with Cr, whereas the cell interiors are enriched with Fe, Co, and Ni. Post-annealing at 1000 °C promotes the formation of equiaxed grained microstructures (i. e., recrystallization), and simultaneously erases the elemental segregation. Such a simple phase structure and uniform elemental distribution leads to a higher corrosion potential and a lower corrosion current density, indicating an enhanced corrosion resistance.

CRediT authorship contribution statement

Qi Zhu: Conceptualization, Methodology, Data curation, Writing – original draft, Writing – review & editing. **Yu Liu:** Writing – review & editing. **Chunyang Zhang:** Conceptualization, Funding acquisition, Writing – review & editing.

Declaration of Competing Interest

The authors declare that they have no known competing financial interests or personal relationships that could have appeared to influence the work reported in this paper.

Acknowledgements

The authors acknowledge the financial support from Shenyang Science and Technology Plan (code: 201937).

Appendix A. Supplementary data

Supplementary data to this article can be found online at https://doi.org/10.1016/j.matlet.2022.132133.

References

- [1] J.W. Yeh, S.K. Chen, S.J. Lin, J.Y. Gan, T.S. Chin, T.T. Shun, C.H. Tsau, S.Y. Chang, Adv. Eng. Mater. 6 (5) (2004) 299–303.
- [2] P.J. Shi, W.L. Ren, T.X. Zheng, Z.M. Ren, X.L. Hou, J.C. Peng, P.F. Hu, Y.F. Gao, Y. B. Zhong, P.K. Liaw, Nat. Commun. 10 (2019).
- [3] T. Fujieda, M. Chen, H. Shiratori, K. Kuwabara, K. Yamanaka, Y. Koizumi, A. Chiba, S. Watanabe, Addit. Manuf. 25 (2019) 412–420.
- [4] H. Cheng, Z. Pan, Y. Fu, X. Wang, Y. Wei, H. Luo, X. Li, J. Electrochem. Soc. 168 (11) (2021), 111502.
- [5] Y. Fu, J. Li, H. Luo, C. Du, X. Li, J. Mater. Sci. Technol. 80 (2021) 217-233.
- [6] W. Li, P. Liu, P.K. Liaw, Mater. Res. Lett. 6 (4) (2018) 199-229.
- [7] J. Menghani, A. Vyas, P. Patel, H. Natu, S. More, Mater. Today: Proc. 38 (2021) 2824–2829.
- [8] P. Zhang, Z. Li, H. Liu, Y. Zhang, H. Li, C. Shi, P. Liu, D. Yan, J. Manuf. Process. 76 (2022) 397–411.
- [9] H. Zhang, Y.-Z. He, Y. Pan, S. Guo, J. Alloys Compd. 600 (2014) 210-214.
- [10] C. Ni, Y. Shi, J. Liu, G. Huang, Opt. Laser Technol. 105 (2018) 257-263.
- [11] X.-W. Qiu, M.-J. Wu, C.-G. Liu, Y.-P. Zhang, C.-X. Huang, J. Alloys Compd. 708 (2017) 353–357.
- [12] G. Jin, Z. Cai, Y. Guan, X. Cui, Z. Liu, Y. Li, M. Dong, D. Zhang, Appl. Surf. Sci. 445 (2018) 113–122.
- [13] X.J. Jiang, S.Z. Wang, H. Fu, G.Y. Chen, Q.X. Ran, S.Q. Wang, R.H. Han, Mater. Lett. 308 (2022).
- [14] Q. Ye, K. Feng, Z. Li, F. Lu, R. Li, J. Huang, Y. Wu, Appl. Surf. Sci. 396 (2017) 1420–1426.
- [15] Z. Wu, H. Bei, G.M. Pharr, E.P. George, Acta Mater. 81 (2014) 428-441.
- [16] Y. Brif, M. Thomas, I. Todd, Scr. Mater. 99 (2015) 93-96.
- [17] Z. Wu, H. Bei, F. Otto, G.M. Pharr, E.P. George, Intermetallics 46 (2014) 131–140.
- [18] Z. Sun, X.P. Tan, M. Descoins, D. Mangelinck, S.B. Tor, C.S. Lim, SCR Mater. 168 (2019) 129–133.
- [19] Y. Xiong, W.H. Hofmeister, Z. Cheng, J.E. Smugeresky, E.J. Lavernia, J. M. Schoenung, Acta Mater. 57 (18) (2009) 5419–5429.
- [20] P.A. Hooper, Addit. Manuf. 22 (2018) 548–559.
- [21] K.Y. Tsai, M.H. Tsai, J.W. Yeh, Acta Mater. 61 (13) (2013) 4887-4897.